HHS Public Access

Author manuscript

Anal Chem. Author manuscript; available in PMC 2018 May 02.

Published in final edited form as:

Anal Chem. 2017 May 02; 89(9): 4855–4862. doi:10.1021/acs.analchem.6b04491.

Nanofluidic Devices with 8 Pores in Series for Real-Time, Resistive-Pulse Analysis of Hepatitis B Virus Capsid Assembly

Panagiotis Kondylis[1], **Jinsheng Zhou**[1], **Zachary D. Harms**[1], **Andrew R. Kneller**[1], **Lye Siang Lee**[2], **Adam Zlotnick**[2], and **Stephen C. Jacobson**[1,*]

[1]Department of Chemistry, Indiana University, Bloomington, IN 47405

[2]Department of Molecular and Cellular Biochemistry, Indiana University, Bloomington, IN 47405

Abstract

To improve the precision of resistive-pulse measurements, we have used a focused ion beam instrument to mill nanofluidic devices with 2, 4, and 8 pores in series and compared their performance. The in-plane design facilitates the fabrication of multiple pores in series, which, in turn, permits averaging of the series of pulses generated from each translocation event. The standard deviations (σ) of the pulse amplitude distributions decrease by 2.7-fold when the average amplitudes of eight pulses are compared to the amplitudes of single pulses. Similarly, standard deviations of the pore-to-pore time distributions decrease by 3.2-fold when the averages of the seven measurements from 8-pore devices are contrasted to single measurements from 2-pore devices. With signal averaging, the inherent uncertainty in the measurements decreases; consequently, the resolution (mean/σ) improves by a factor equal to the square root of the number of measurements. We took advantage of the improved size resolution of the 8-pore devices to analyze in real time the assembly of Hepatitis B Virus (HBV) capsids below the pseudo-critical concentration. We observe that abundances of assembly intermediates change over time. During the first hour of the reaction, the abundance of smaller intermediates decreased, whereas the abundance of larger intermediates with sizes closer to a T = 4 capsid remained constant.

Table of Contents

*Corresponding Author and Contact Information: Stephen C. Jacobson, Department of Chemistry, Indiana University, 800 E. Kirkwood Ave., Bloomington, IN 47405-7102, phone: +1-812-855-6620, jacobson@indiana.edu.

Supporting Information Available. Reducing SDS-PAGE of Cp149, TEM image of virus capsids assembled from Cp149 dimer, pulse sequences from an 8-pore device, pulse sequences from 2-and 4-pore devices, and histogram and corresponding fitted data of a 1:1 mixture of T = 3 and T = 4 capsids. This material is available free of charge via the Internet at http://pubs.acs.org.

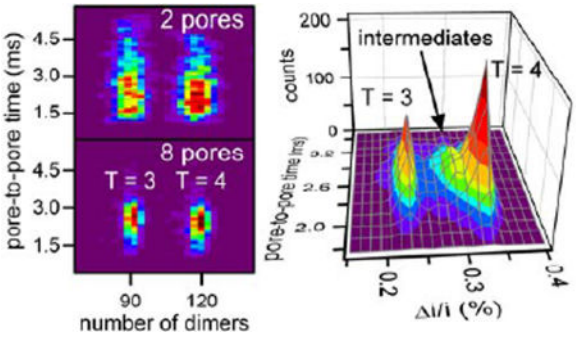

Keywords

Nanofluidics; Resistive-Pulse Sensing; Multi-Pore Sensing; Hepatitis B Virus; Self-Assembly; Assembly Intermediates

Understanding virus capsid assembly is critical for the development of new biomaterials[1,2] and assembly-directed antiviral drugs.[3–5] Two components are critical features of viruses, the viral genome (DNA or RNA) and the virus capsid, which functions as the protective package of the genome. In about half of known virus families, the capsid is a spherical complex arranged with icosahedral geometry.[6] Icosahedral geometry requires 60 equivalent asymmetric units, which may in turn be constructed of several quasi-equivalent copies of the capsid protein(s).[7] To approach the complicated virus self-assembly reactions, different models have been developed.[8–12] Simulations have led to experimentally verified predictions that assembly is generally based on weak interactions between multivalent subunits.[13–14] Experimental observations indicate that in some cases assembly involves specific intermediates (incomplete capsids), suggesting a limited number of assembly paths.[15–19] Thus, a key factor for the development of thermodynamic and kinetic models for virus capsid assembly is the better characterization of the assembly intermediate species.

Hepatitis B Virus (HBV) capsid assembly has been studied as a model system for understanding the virus self-assembly mechanism.[14] Analysis of HBV assembly has also been of significant interest due to its threat to public health; according to the World Health Organization (WHO), complications caused by the HBV result in 500,000–700,000 deaths annually.[20–21] HBV is an enveloped double-stranded DNA virus. During HBV assembly, the homodimeric core protein (Cp) forms capsids with T = 4 symmetry (~90% abundance, 120 dimer units, 38 nm diameter) and T = 3 symmetry (~10% abundance, 90 dimer units, 34 nm diameter).[22] The HBV capsid assembly reaction can be triggered in vitro by the dilution of the Cp149 dimer (a truncated version of the 183-residue core protein that is missing the RNA-binding domain) into NaCl solutions at room temperature without the presence of nucleic acid or polyanion template.[23] Truncation of the core protein,[23] concentrations of core protein dimer and salt,[15] and degree of dimer oxidization[22] are factors that affect the ratio of T = 3 and T = 4 capsids formed during capsid assembly. The assembly reaction is characterized by a pseudo-critical concentration, where the concentration of dimers in the capsid equals the concentration of the free dimer in the reaction solution.[13] At 1 M NaCl and room temperature, the pseudo-critical concentration of HBV assembly is 0.5 μM dimer.

Unlike a true critical concentration, assembly is observed in vitro well below the pseudo-critical concentration.[8,15]

Ideally, an analytical method for the characterization of the reaction products of virus assembly would measure single particles in biologically relevant solutions, at biologically relevant concentrations, and in real time. To date, several methods are used to study virus assembly. Size exclusion chromatography (SEC)[13] quantifies dimer and virus capsids in equilibrium, but has poor size resolution. Light scattering methods,[14,24,25] that offer good temporal resolution, report only the average molecular mass. Fluorescence correlation spectrometry[26] has single particle sensitivity, but is limited to very low concentrations. Charge detection mass spectrometry (CD-MS)[17] measures megadalton masses with high resolution, and native ion mobility mass spectrometry (IM-MS) [27] returns information about the masses, shapes, and structures of the self-assembly products. However, because volatile buffers are needed for electrospray ionization, both CD-MS and IM-MS are not compatible with typical assembly buffers. In addition, the measurement procedure does not take place in solution, so assumptions about the desolvation process of the virus capsids are made.

Resistive-pulse sensing[28] is a rapid, single particle analysis method that is used for the analysis of viruses in solution.[15,29–33] In a resistive-pulse experiment, current pulses are recorded as particles displace electrolyte from nanopores. Two approaches are possible for enhancing resolution of resistive-pulse measurements. The first approach is to pass particles back and forth through a single nanopore (i.e., a ping-pong experiment). These ping-pong experiments improved DNA measurements[34–36] and measurements of the size of gold and polystyrene nanoparticles.[37–38] However, the longer acquisition time required for ping-pong experiments is a drawback for real time analysis of virus assembly, especially when the measurement time is comparable to the reaction time.

A second approach to enhance the resolution is the fabrication of nanofluidic devices with multiple pores connected in series. The fabrication of long nanochannels separated by nodes (‘node-pore sensing’) results in a unique signal pattern, used to improve the detection capabilities of resistive-pulse sensing platforms.[39] Devices with two pores in series were used to signal average the amplitudes of two current pulses to better discriminate particle sizes.[31] These two-pore devices also return the electrophoretic mobilities of HBV capsids[30–31] and DNA molecules[40] from the poreto-pore time measurements. More recently, we employed 2-pore devices for the real time analysis of HBV assembly.[15] Although the T = 3 and T = 4 capsid distributions are well resolved in this study, the resolution achieved was not sufficient to permit observation of changes in specific size ranges of assembly intermediates.

Here, with a focused ion beam (FIB) instrument, we milled nanofluidic devices that had 2, 4, and 8 pores in series for the measurement of HBV capsids. The in-plane architecture of these devices facilitates the fabrication of multiple pores in series and the integration of the nanopores with microfluidic components. With T = 3 and T = 4 capsid standards, we measured pulse amplitudes and pore-to-pore times and demonstrated how the resolution (mean/σ) increased with the number of pores. Moving from 2 to 8 pores in series yielded decreases in the standard deviation of the pulse amplitude and pore-to-pore time

distributions of 2.2 and 3.2 times, respectively. Interestingly, the T = 3 and T = 4 capsids had similar, but not identical electrophoretic mobilities. With the improved resolution of the 8-pore device, we monitored in real time the assembly of HBV capsids and their intermediates at 0.40 μM of dimer in 1 M NaCl. For the characterization of the assembly intermediates, the data were fitted with a program based on the Monte Carlo method. Over the 1 h reaction, populations of T = 3 capsids (90 dimers) and T = 4 capsids (120 dimers) increased. For the incomplete capsids, the abundance of intermediates 92 to 104 dimers significantly decreased, whereas the abundance of intermediates from 105 to 117 dimers remained constant.

Experimental Section

Materials

We purchased D263 glass substrates coated with 120 nm of chromium and 530 nm of AZ1518 photoresist from Telic Co.; uncoated D263 glass substrates from Precision Glass & Optics; No. 1.5 coverslips from VWR, Inc.; Microposit S1813 positive-tone photoresist and MF-319 developer from MicroChem Corp.; chromium etchants 1020 and 8002-A and buffered oxide etchant (BOE) from Transene Co., Inc.; sodium chloride from Mallinckrodt; ammonium hydroxide from J.T Baker; Anotop 10 syringe filters from Whatman GmbH; and 353NDT Epoxy from Epoxy Technology, Inc. All other chemicals were purchased from Sigma-Aldrich Co.

Virus Capsids

HBV capsids were assembled from core protein dimers (Cp149 dimer, 34 kDa) that were expressed in *E. coli* and purified as described previously.[41] For the characterization of the multi-pore nanofluidic devices, T = 3 and T = 4 capsids were purified after assembly on a 10% – 40% (w/v) continuous sucrose gradient in 50 mM 4-(2-hydroxyethyl)-1-piperazine-ethanesulfonic acid (HEPES; pH 7.5) with 0.3 M NaCl that was centrifuged for 6 h at 150,000 g.[42] For the assembly experiments, the dimer was used without further purification. Figure S1a in the Supporting Information shows a reducing SDS-PAGE of 6 μg Cp149, which runs as a 17 kDa monomer under reducing conditions. The high-purity dimer sample led to properly formed T = 3 and T = 4 capsids, which are shown in the transmission electron microscope (TEM) image in Figure S1b in the Supporting Information. For the TEM images, capsids were assembled from 5 μM dimer in 1 M NaCl, and the assembly products were adsorbed to glow-discharged carboncoated grids (EM Sciences), stained with 2% uranyl acetate, and analyzed with a TEM (JEM-1010, JEOL Ltd.) operated at 80 kV.

Fabrication of Nanofluidic Devices

For the substrates without the chromium and the photoresist layers, a 120 nm thick layer of chromium was deposited with a thermal evaporator (BOC Edwards Auto 306 Vacuum Coating System) and a 3 μm thick layer of S1813 photoresist was spin-coated onto the chromium layer. To fabricate the V-shaped microchannels in Figure 1a, positive-tone UV photolithography and wet etching techniques were used.[31] The depth of the microchannels was determined with a stylus-based profiler (Dektak 6M, Veeco Instruments, Inc.), and the channel width was determined with an optical microscope (Nikon Eclipse TE2000-E).

To fabricate the nanochannels and nanopores, we used a focused ion beam (FIB) instrument (Auriga 60, Carl Zeiss, GmbH) controlled by the Nano-Pattering and Visualization Engine (NPVE; FIBICS, Inc.).[31] The nanochannels in Figure 1c,d were milled with a 30 kV beam at 50 pA. The side nanochannels were milled with a dose of 1 nC/μm^2, and the bridge and pore-to-pore nanochannels were milled with a dose of 0.5 nC/μm^2. To connect the nanochannels, we milled the nanopores as a single line with a 30 kV beam at 20 pA and a dose of 0.01 μC/μm. During the FIB milling, an electron flood gun (FG 15/40, SPECS, GmbH), operated at 5 eV and 20 μA, compensates for the build-up of positive charge on the substrate surface. Dimensions of the nanochannels and nanopores were measured with an atomic force microscope (AFM; MFP-3D, Asylum Research, Inc.) and the scanning electron microscope (SEM) on the FIB instrument.

For bonding of the devices, the substrates and No. 1.5 cover slips were cleaned in 1 M NaOH for 15 min, sonicated in ultrapure water for 10 min, and brought into contact with each other while still wet. The devices were dried overnight at 90 °C and annealed at 545 °C for 12 h. To hold samples and buffers and make electrical contact to them, glass reservoirs were epoxied over the access holes.

Resistive-Pulse Measurements

To rinse the devices, the two reservoirs in the middle were filled with solution, and vacuum was applied at the reservoirs on the ends. Before the first use, each device was rinsed with H_2O for 10 min, 0.1 M NaOH for 15 min, H_2O for 5 min, and buffer solution (50 mM HEPES, 1 M NaCl) for 5 min. All solutions, except for the samples, were filtered with 20 nm syringe filters. Finally, the sample was loaded into one of the two reservoirs in the middle, and vacuum was applied to the corresponding end reservoir for 30 s.

We conducted resistive-pulse measurements inside a stainless steel Faraday cage covered with wedge foam. An Axopatch 200B (Molecular Devices, Inc.) was used to apply the potential between the two reservoirs in the middle through Ag/AgCl electrodes and to record the current. For the 2-and 4-pore devices, the reservoir filled with the sample was connected directly to ground. For the 8-pore devices, a battery set at 900 mV was connected in series with the circuit, with which potentials > 1 V were applied.

Measurements on all the devices were taken with a baseline current of ~17 nA. The applied potential was in the range of 490–500 mV for the 2-pore devices, 800–890 mV for the 4-pore devices, and 1460–1900 mV for the 8-pore devices. All data were collected with a sampling frequency of 40 kHz, a gain of $\alpha = 0.5$, a head stage amplification of $\beta = 1$, and a filter frequency of 10 kHz.

To calibrate each nanofluidic device, we measured the pulse amplitudes of separate solutions of purified T = 3 and T = 4 capsids in 50 mM HEPES buffer (pH = 7.5) with 1 M NaCl. Consequently, devices with varying numbers of pores and with small differences in pore dimensions are easily calibrated, and data can be quantitatively compared across all devices and experiments. For assembly reactions, Cp149 dimer was brought to an initial concentration of 0.40 μM in 50 mM HEPES buffer (pH = 7.5) with 1 M NaCl and loaded onto the device. A period of ~100 s elapsed between the initial mixing of the dimer into 1 M

NaCl and the start of the resistive-pulse measurements. Data were collected continuously for 60 min.

Data Analysis

To determine the pulse amplitudes and pore-to-pore times, we imported the raw data into MatLab R2014a (Mathworks, Inc.) and used a modified version of Open Nanopore 1.2 to analyze the raw data and determine the pulse amplitude (Δi), pulse width (w), and average baseline current adjacent to each pulse.[43] Pore-to-pore times (i.e., time segments between pulses) were tabulated and plotted on a logarithmic scale to reveal two distributions: correlated times for individual capsids and uncorrelated times from different capsids. A Gaussian function was fitted to the pore-to-pore time distribution with Origin Pro 2015 (OriginLab Corp.), and the standard deviation of the fitted function was used as a selection criterion for correlated sets of pulses. Uncorrelated events, e.g., series of current pulses produced by two particles inside the pores simultaneously, were not analyzed further or included in the amplitude and pore-to-pore time distributions. The average pulse amplitude from each set of pulses was divided by the average baseline current adjacent to each pulse to calculate normalized pulse amplitude (Δi/i).

For the fitting of the assembly data at 0.40 μM dimer, Δi/i values of each data set were plotted as a single histogram, and the standard deviation of the distribution that corresponded to T = 3 capsids was determined. The data were parsed into 15-min intervals and analyzed further. Δi/i values of the means of the T = 3 and T = 4 capsid distributions were determined from the amplitude histograms for each 15 min interval. The Δi/i values were imported into the MatLab program, and Gaussian distributions were fitted to the corresponding amplitude histograms based on the Monte Carlo method. The bin size used for the fitting was 1.2 times smaller than the bin size that corresponds to a single dimer, whereas the standard deviation (σ) for each Gaussian distribution was calculated by equation 1 as:

$$\sigma = \sigma_{T=3} \times \left(0.1 \times \frac{\text{number of dimers} - 90}{30} + 1\right) \quad (1)$$

where the $\sigma_{T=3}$ is the standard deviation of the peak that corresponds to a T = 3 capsid distribution. Amplitudes and σ of the fitted distributions were used to calculate the abundances of T = 3 capsids, T = 4 capsids, and intermediate species

Results and Discussion

Device Design

To characterize the multi-pore devices, we fabricated two 2-pore, two 4-pore, and two 8-pore devices. Figure 1a shows a schematic of these devices, which consists of two V-shaped microchannels connected through a series of nanochannels and nanopores milled as a single line (Figure 1c). Across all the devices, the nanopores were 291 ± 11 nm long, 58 ± 7 nm wide, and 66 ± 3 nm deep. In comparison, T = 4 capsids have an external diameter of 38 nm, measured by light scattering. The pore-to-pore nanochannels were 503 ± 7 nm long, 317 ± 4

nm wide, and 130 ± 3 nm deep. The side nanochannels were 498 ± 8 nm wide and 264 ± 4 nm deep. The V-shaped microchannels were 35.0 ± 0.4 μm wide and 9.7 ± 0.1 μm deep. For one of the 4-pore devices and both 8-pore devices, two bridge nanochannels, which were 304 ± 12 nm long and had the same width and depth as the pore-to-pore nanochannels, were added to the design (Figure 1d). Without the bridge nanochannels, the two nanopores on the ends adjacent to the side nanochannels have larger lateral dimensions, because the increased surface area on the deeper sides of the pores results in higher sputtering rates during the FIB milling. The above dimensions of the nanopores, nanochannels, and microchannels are averages across all six devices, and the deviations are due to the variability in the fabrication process from device to device and the measurement of those dimensions.

Measurement of Pulse Amplitude

T = 3 capsids (1 nM), T = 4 capsids (1 nM), and a 1:1 mixture of T = 3 and T = 4 capsids (0.5 nM each) were measured on each device. A positive potential is applied across the nanochannels, and the axial electric field drives the negatively charged HBV particles through the nanopores electrophoretically in the anodic direction. Because the experiments are conducted in 1 M NaCl, the electroosmotic flow in the nanochannels and nanopores is suppressed and ~10-fold lower in magnitude than the electrophoretic transport of the capsids in the opposite direction. As the virus capsid migrates electrokinetically through a nanopore and displaces electrolyte, the resistance in the pore increases, and a transient change in current (pulse) is recorded. A schematic representation of the measurement procedure is depicted in Figure 1b. The average sampling time was ~20 min for each experiment, which corresponded to > 800 capsid translocation events. In Figure 2a, a 3-s current trace from the analysis of a 1:1 mixture of T = 3 and T = 4 capsids on an 8-pore device is illustrated. Each pulse sequence corresponds to the translocation of a single capsid through the nanopores and consists of eight pulses (Figure 2b). Pulse sequences from virus capsids transiting 2-and 4-pore devices are shown in Figure S3 in the Supporting Information. Differences in the amplitudes of the 8 pulses are attributed to the inherent uncertainty in each measurement and to variability in the pore dimensions that arises during fabrication (Figure S2 in the Supporting Information).

Pulse amplitudes (Δi) from each pulse sequence (2, 4, or 8) were averaged together and normalized by the baseline current (Δi/i). The means of the Δi/i distributions for T = 4 capsids were 0.51% ± 0.01%, 0.48% ± 0.01%, and 0.32% ± 0.02% for the 2-, 4-, and 8-pore devices, respectively. As more nanopores and pore-to-pore nanochannels are added to the design, the total resistance of the nanofluidic device increases, and consequently, the percent of the potential drop across each of the nanopores decreases. The shape of the nanopore was approximated to be rectangular, and the potential drops across each nanopore were calculated to be ~27% for the 2-pore devices, ~18% for the 4-pore devices, and ~10% for the 8-pore devices.

Figure 3a shows the significant improvement in particle size resolution achieved with the 8-pore devices. As the number of nanopores connected in series increases, the distributions of the pulse amplitudes for the T = 3 and T = 4 capsids become narrower. The histograms of the pulse amplitudes were fitted with Gaussian functions, and the standard deviation (σ) was

divided by the distribution mean to determine the relative standard deviation (RSD). In Figure 3b, RSDs for the amplitude distributions of the T = 3 and T = 4 capsids from 2-, 4-, and 8-pore devices are plotted as a function of the number of measurements. Each point in the graph corresponds to six different experiments (three with each device). From the 2-, 4-, and 8-pore devices, we also extracted measurements for the equivalent of 1 pore, 1 to 3 pores, and 1 to 7 pores, respectively, to better understand the trends for intermediate numbers of pores.

With the 8-pore devices, RSDs of less than 3.0% and 2.5% are reported for T = 3 and T = 4 capsids, respectively. Interestingly, the RSDs from the 2-pore devices are comparable to the RSDs from the 4-and 8-pore devices when only the first two pulses from each pulse sequence are averaged. In the same manner, the RSDs from the 4-pore devices are similar to the RSDs from the 8-pore devices when only four pulses from each pulse sequence are averaged. This observation leads to the conclusion that the inherent uncertainty in each measurement remains constant, despite the fact that some signal amplitude is lost with the 4- and 8-pore devices due to the increased resistance. In other words, the standard deviation and resolution of the pulse amplitude distribution decreases and increases, respectively, by a factor proportional to the square root of the number of pores, even when devices with different numbers of pores are compared. We expect to observe a 2.8-fold decrease in the standard deviation in the pulse amplitude distribution when the amplitudes of eight pulses are averaged and compared to the amplitudes of single pulses. Indeed, we see a 2.7-fold decrease in the standard deviations, which suggests the inherent uncertainty of the measurement contributes more to the measurement error than the slight variations in the nanopore dimensions. Thus, although the pulse amplitude decreases when multiple pores are connected in series, the 8-pore devices are preferred as long as particles can be detected, and the pulse amplitude does not fall below the threshold used for the data analysis. For the analysis of HBV capsids on 8-pore devices, the smaller T = 3 capsids were easily distinguished from the noise; the estimated limit of detection is ~40 dimers.

Measurement of Pore-to-Pore Times

Because the T = 3 and T = 4 capsids are formed from the same protein, their electrophoretic mobilities should be similar. To analyze the pore-to-pore times of T = 3 and T = 4 capsids, the pulse amplitudes were used as the criterion to determine which pulse sequences corresponded to T = 3 or T = 4 capsids. As with the pulse amplitudes, averaging of the pore-to-pore times resulted in decreased RSDs of the distributions. With the enhanced resolution of the electrophoretic mobility measured with the 8-pore devices, the pore-topore time distributions of T = 3 and T = 4 capsids actually have different means (Figure 4a). This difference in pore-to-pore times was not previously observed on 2-pore devices[31] due to the insufficient resolution. From the data in Figure 4a, the average velocities of the T = 3 and T = 4 capsids are 1.8×10^{-2} and 2.0×10^{-2} cm/s in the pore-to-pore nanochannels, respectively. Based on these velocities and the electroosmotic flow in 1 M NaCl,[44] the average electrophoretic mobilities of T = 3 and T = 4 capsids are 7.3×10^{-5} and 7.0×10^{-5} $cm^2V^{-1}s^{-1}$, respectively. These mobilities are in agreement with the values measured previously on 2-pore devices[31] and with mobilities calculated for similarly sized viruses measured by capillary electrophoresis.[45]

In T = 3 capsids, the 90 dimers are arranged as 12 pentamers and 20 hexamers, whereas in T = 4 capsids, the 120 dimers are arranged as 12 pentamers and 30 hexamers. If hexamers have higher surface charge or pentamers shield part of the charge because of the differences in the angle between the dimer units, then the surface charge per unit area will be higher on the T = 4 capsids than the T = 3 capsids. In addition, the center of each hexamer has a pore with a diameter of 2–3 nm.[23] These pores allow transient exposure of the C-terminal carboxyl of the core protein.[46] Also, the higher porosity per unit area of T = 4 capsids could result in a decreased hydrodynamic drag. Thus, surface charge, hydrodynamic drag, or both could result in the observed difference between the mobilities of T = 3 and T = 4 capsids.

When the pore-to-pore time is measured only once, the measurements exhibit a log-normal distribution,[31] because some of the capsids interact with the nanochannels during translocation. Consequently, we had to use the logarithm of the pore-to-pore times to calculate the RSD for different devices. However, as seen in Figure 4a, the use of the logarithm is not necessary with the 8-pore devices because the pore-to-pore times are measured seven times for each particle, and any interactions of the particles with the nanochannels are averaged. In Figure 4b, the RSDs of the T = 3 and T = 4 capsid distributions are plotted. T = 3 and T = 4 capsids have very similar electrophoretic mobilities; consequently, RSDs of pore-to-pore times for T = 3 and T = 4 capsids are almost identical for the same number of measurements. When we compare seven measurements to one measurement, we anticipate a 2.6-fold decrease in the width of the pore-topore time distribution, but observe a 3.2-fold decrease. The higher than expected improvement stems primarily from the distributions shifting from log-normal for a single measurement to normal for seven measurements.

HBV Assembly below the Pseudo-Critical Concentration

For the real time analysis of HBV assembly, two 8-pore devices were tested. The dimensions of these devices were nominally the same as those devices described above. In vitro assembly of dimer can be induced by increasing the ionic strength. Here, the assembly reaction was initiated off-chip by the dilution of the dimer solution to a final concentration of 0.40 μM in 50 mM HEPES buffer with 1 M NaCl, and the reaction solution was continuously monitored for 1 h. The same experiment was repeated three times in total, on different days and with different dimer solutions.

The assembly data were parsed into 15-min intervals and analyzed; each interval included ~750 capsids. Two representative histograms of the pulse amplitudes from 0 to 15 min and 45 to 60 min of the data acquisition are illustrated in the Figures 5a and 5b, respectively. As seen in the raw data, the abundance of the assembly intermediates decreased over time, and the intermediates remaining in the reaction solution shifted to larger sizes. As predicted from simulations, the population of intermediates shifts over time, favoring larger and more stable species.[8,47–48] In this study, intermediates with sizes in the range from ~40 dimers (limit of detection) to the size of T = 3 capsids (90 dimers) were not detected in appreciable amounts, which suggests they are short-lived or found only at low concentration. Previous studies with mass spectrometry have shown the presence of small oligomers with sizes up to 40 dimers, but under different reaction conditions (e.g., protein concentration, buffer, and pH).[27,49]

The pulse amplitudes are proportional to the protein volume of HBV capsids.[31] Thus, to determine and quantify the intermediates present in the reaction solution, we developed a fitting program based on the Monte Carlo method in which Gaussian distributions are fitted to the raw data. The standard deviation of the pulse amplitude distribution for T = 3 capsids was used as input to the program because assembly intermediates close to the T = 3 capsids were not present and did not widen the distribution. The standard deviations of the other distributions were based on measurements of the 1:1 mixture of T = 3 and T = 4 capsids and was 1.1 times larger for T = 4 than T = 3 capsids. We assumed the standard deviation of the Gaussian distributions changed linearly with the number of dimers (see Equation 1). Unlike the T = 3 capsid distribution, the T = 4 capsid distribution from the assembly reactions was always wider than the distribution of the standard solutions, which indicated the presence of unresolved intermediate species with sizes close to T = 4 capsids. To test the fitting program, histograms from 1:1 mixtures of T = 3 and T =4 capsid standards were analyzed. Indeed, both T = 3 and T = 4 capsid distributions were fitted by single Gaussians (Figure S4 in the Supporting Information).

For the capsid assembly reaction, Figure 5a,b shows the results of the fitting algorithm for the pulse amplitude histograms, which consist of the fitted line and heights of the individual Gaussian distributions. To quantify the results of the fitting program, we assigned the Gaussian distributions with means equal to 90 ± 1 dimers as T = 3 capsids and 120 ± 2 dimers as T = 4 capsids; the intermediates were separated into the ranges of 92–104 dimers and 105–117 dimers. The heights and corresponding standard deviations of each Gaussian distribution were used to determine the area of each distribution and, subsequently, to calculate the abundance of each group noted above. Figure 6 shows the abundances of T = 3 and T = 4 capsids increase slightly over time. In addition, a clear decrease in the abundance of intermediates in the range of 92–104 dimers is illustrated in Figure 7a. On the contrary, intermediate species in the range of 105–117 dimers remained constant during the experiment (Figure 7b). This observation suggests that smaller intermediates evolved into larger intermediates, which in turn, complete into T = 4 capsids.

Conclusion

We show that 8-pore devices are an excellent tool for the real-time analysis of virus assembly. The enhanced particle size resolution combined with the rapid acquisition time enabled the real time observation of changes in specific size ranges of intermediate species formed during the assembly of HBV not accessible by other methods. Thus, resistive-pulse sensing on multi-pore devices complements information from other techniques and offers new insights into the self-assembly mechanism. The primary advantage of the multi-pore measurements, compared to the cycling of the particles back-and-forth through a single pore, is that the flow is kept unidirectional during the measurement process. Thus, 8-pore devices can be integrated in designs with on-chip mixing tees and pressure driven flow. This approach will allow the sampling of early time points during the assembly reaction and provide information about the lag phase of the HBV assembly reaction, which corresponds to the time required for the building of a pipeline of intermediates,[50–51] when the most dramatic changes are taking place.

Supplementary Material

Refer to Web version on PubMed Central for supplementary material.

Acknowledgments

This work was supported in part by NIH R01 GM100071 and NSF CHE-0923064. The authors thank the Indiana University Nanoscale Characterization Facility for use of its instruments.

References

1. Douglas T, Young M. Science. 2006; 312:873–875. [PubMed: 16690856]
2. Dragnea B. Nat. Mater. 2008; 7:102–104.
3. Deres K, et al. Science. 2003; 299:893–896. [PubMed: 12574631]
4. Stray SJ, Bourne CR, Punna S, Lewis WG, Finn MG, Zlotnick A. Proc. Natl. Acad. Sci. U. S. A. 2005; 102:8138–8143. [PubMed: 15928089]
5. Prevelige PE. J. Mol. Biol. 2011; 410:634–640. [PubMed: 21762804]
6. Fields, BN., Knipe, DM., Howley, PM., Chanock, RM., Melnick, JL., Monath, TP., Roizman, B., Straus, SE. Virology. 3. Lippincott-Raven Publishers; Philadelphia: 1996.
7. Caspar DLD, Klug A. Cold Spring Harbor Symp. Quant. Biol. 1962; 27:1–24. [PubMed: 14019094]
8. Zlotnick A. J. Mol. Biol. 1994; 241:59–67. [PubMed: 8051707]
9. Zhang TQ, Schwartz R. Biophys. J. 2006; 90:57–64. [PubMed: 16214864]
10. Hagan MF, Chandler D. Biophys. J. 2006; 91:42–54. [PubMed: 16565055]
11. Zandi R, van der Schoot P, Reguera D, Kegel W, Reiss H. Biophys. J. 2006; 90:1939–1948. [PubMed: 16387781]
12. Perlmutter JD, Hagan MF. Annu. Rev. Phys. Chem. 2015; 66:217–239. [PubMed: 25532951]
13. Ceres P, Zlotnick A. Biochemistry. 2002; 41:11525–11531. [PubMed: 12269796]
14. Zlotnick A, Johnson JM, Wingfield PW, Stahl SJ, Endres D. Biochemistry. 1999; 38:14644–14652. [PubMed: 10545189]
15. Harms ZD, Selzer L, Zlotnick A, Jacobson SC. ACS Nano. 2015; 9:9087–9096. [PubMed: 26266555]
16. Johnson JM, Tang JH, Nyame Y, Willits D, Young MJ, Zlotnick A. Nano Lett. 2005; 5:765–770. [PubMed: 15826125]
17. Pierson EE, Keifer DZ, Selzer L, Lee LS, Contino NC, Wang JCY, Zlotnick A, Jarrold MF. J. Am. Chem. Soc. 2014; 136:3536–3541. [PubMed: 24548133]
18. Tresset G, Decouche V, Bryche JF, Charpilienne A, Le Coeur C, Barbier C, Squires G, Zeghal M, Poncet D, Bressanelli S. Arch. Biochem. Biophys. 2013; 537:144–152. [PubMed: 23871846]
19. Tresset G, Le Coeur C, Bryche JF, Tatou M, Zeghal M, Charpilienne A, Poncet D, Constantin D, Bressanelli S. J. Am. Chem. Soc. 2013; 135:15373–15381. [PubMed: 23822934]
20. WHO. Weekly Epidemiological Record. 2004; 79:253–264. [PubMed: 15344665]
21. Selzer L, Zlotnick A. Cold Spring Harbor Perspect. Med. 2015; 5:91–108.
22. Selzer L, Katen SP, Zlotnick A. Biochemistry. 2014; 53:5496–5504. [PubMed: 25102363]
23. Zlotnick A, Cheng N, Conway JF, Booy FP, Steven AC, Stahl SJ, Wingfield PT. Biochemistry. 1996; 35:7412–7421. [PubMed: 8652518]
24. Prevelige PE, Thomas D, King J. Biophys. J. 1993; 64:824–835. [PubMed: 8471727]
25. Chen C, Kao CC, Dragnea B. J. Phys. Chem. A. 2008; 112:9405–9412. [PubMed: 18754598]
26. Borodavka A, Tuma R, Stockley PG. Proc. Natl. Acad. Sci. U. S. A. 2012; 109:15769–15774. [PubMed: 23019360]
27. Uetrecht C, Barbu IM, Shoemaker GK, van Duijn E, Heck AJR. Nat. Chem. 2011; 3:126–132. [PubMed: 21258385]
28. DeBlois RW, Bean CP. Rev. Sci. Instrum. 1970; 41:909–916.

29. Zhou K, Li L, Tan Z, Zlotnick A, Jacobson SC. J. Am. Chem. Soc. 2011; 133:1618–1621. [PubMed: 21265511]
30. Harms ZD, Mogensen KB, Nunes PS, Zhou K, Hildenbrand BW, Mitra I, Tan Z, Zlotnick A, Kutter JP, Jacobson SC. Anal. Chem. 2011; 83:9573–9578. [PubMed: 22029283]
31. Harms ZD, Haywood DG, Kneller AR, Selzer L, Zlotnick A, Jacobson SC. Anal. Chem. 2015; 87:699–705. [PubMed: 25489919]
32. Uram JD, Ke K, Hunt AJ, Mayer M. Angew. Chem. Int. Ed. 2006; 45:2281–2285.
33. McMullen A, de Haan HW, Tang JX, Stein D. Nat. Comm. 2014; 5:4171.
34. Gershow M, Golovchenko JA. Nat. Nanotechnol. 2007; 2:775–779. [PubMed: 18654430]
35. Sen YH, Jain T, Aguilar CA, Karnik R. Lab Chip. 2012; 12:1094–1101. [PubMed: 22298224]
36. Plesa C, Cornelissen L, Tuijtel MW, Dekker C. Nanotechnology. 2013; 24:475101. [PubMed: 24177388]
37. German SR, Hurd TS, White HS, Mega TL. ACS Nano. 2015; 9:7186–7194. [PubMed: 26083098]
38. Edwards MA, German SR, Dick JE, Bard AJ, White HS. ACS Nano. 2015; 9:12274–12282. [PubMed: 26549738]
39. Balakrishnan KR, Anwar G, Chapman MR, Nguyen T, Kesavaraju A, Sohn LL. Lab Chip. 2013; 13:1302–1307. [PubMed: 23386180]
40. Langecker M, Pedone D, Simmel FC, Rant U. Nano Lett. 2011; 11:5002–5007. [PubMed: 21981323]
41. Zlotnick A, Ceres P, Singh S, Johnson JM. J. Virol. 2002; 76:4848–4854. [PubMed: 11967301]
42. Zlotnick A, Palmer I, Kaufman JD, Stahl SJ, Steven AC, Wingfield PT. Acta Crystallogr. Sect. D-Biol. Crystallogr. 1999; D55:717–720.
43. Raillon C, Granjon P, Graf M, Steinbock LJ, Radenovic A. Nanoscale. 2012; 4:4916–4924. [PubMed: 22786690]
44. Haywood DG, Harms ZD, Jacobson SC. Anal. Chem. 2014; 86:11174–11180. [PubMed: 25365680]
45. Kremser L, Bilek G, Blaas D, Kenndler E. J. Sep. Sci. 2007; 30:1704–1713. [PubMed: 17623450]
46. Selzer L, Kant R, Wang JCY, Bothner B, Zlotnick A. J. Biol. Chem. 2015; 290:28584–28593. [PubMed: 26405031]
47. Endres D, Miyahara M, Moisant P, Zlotnick A. Protein Sci. 2005; 14:1518–1525. [PubMed: 15930000]
48. Moisant P, Neeman H, Zlotnick A. Biophys. J. 2010; 99:1350–1357. [PubMed: 20816046]
49. Shepherd DA, Holmes K, Rowlands DJ, Stonehouse NJ, Ashcroft AE. Biophys. J. 2013; 105:1258–1267. [PubMed: 24010669]
50. Katen S, Zlotnick A. Methods Enzymol. 2009; 455:395–417. [PubMed: 19289214]
51. Hagan MF, Elrad OM. Biophys. J. 2010; 98:1065–1074. [PubMed: 20303864]

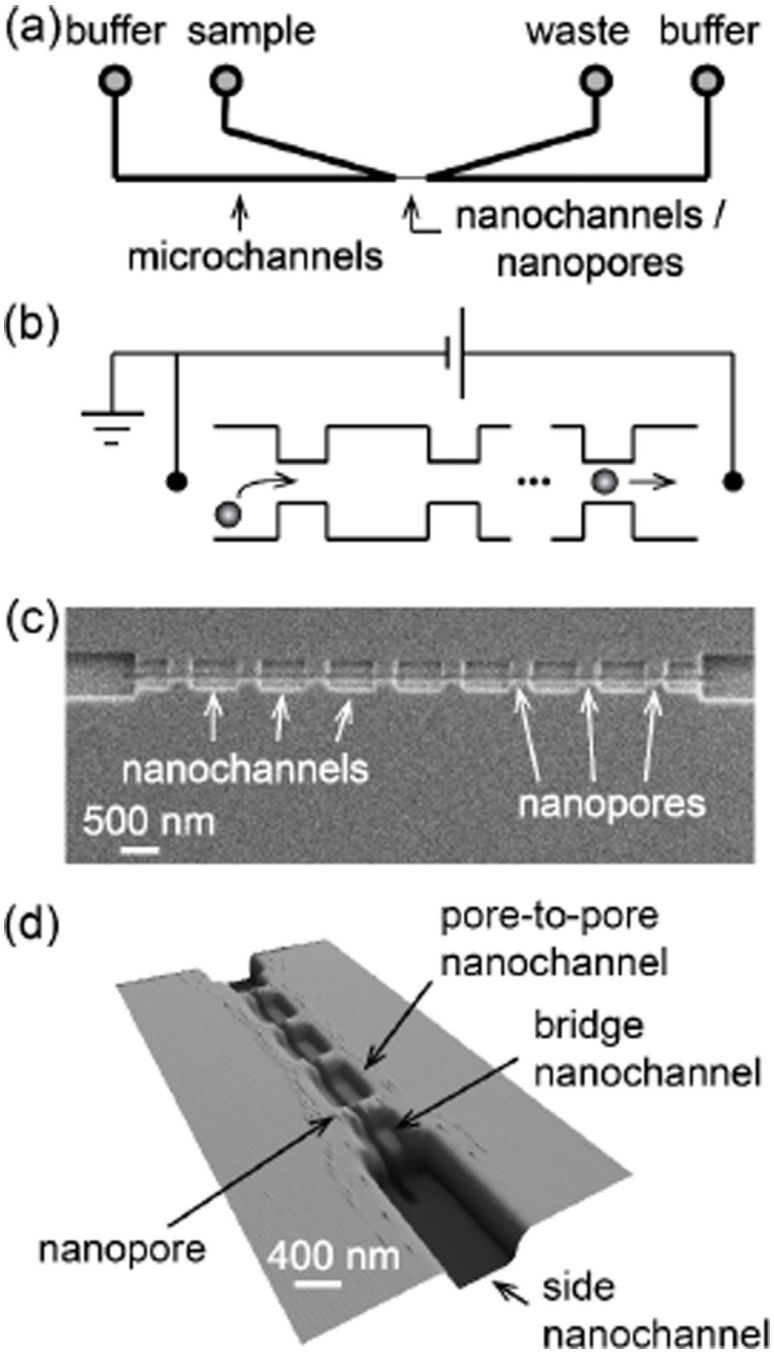

Figure 1.

(a) Schematic of the in-plane nanofluidic device. The in-line series of nanochannels and nanopores bridge the gap between two V-shaped microchannels, which provide fluidic and electrical access to the nanochannels. (b) Schematic of the measurement procedure. As a particle migrates through the nanopore, the resistance in the pore increases, and a transient change in current (pulse) is recorded. (c) Scanning electron microscope (SEM) image of the nanochannel and nanopore region of an 8-pore device. The nanopores are 60 nm wide, 70 nm deep, and 290 nm long, and the pore-to-pore nanochannels are 320 nm wide, 130 nm

deep, and 500 nm long. (d) Atomic force microscope (AFM) image of a 4-pore device. The bridge nanochannel is 320 nm wide, 130 nm deep, and 300 nm long, and the side nanochannels were 500 nm wide and 260 nm deep and varied in length depending on the number of pores.

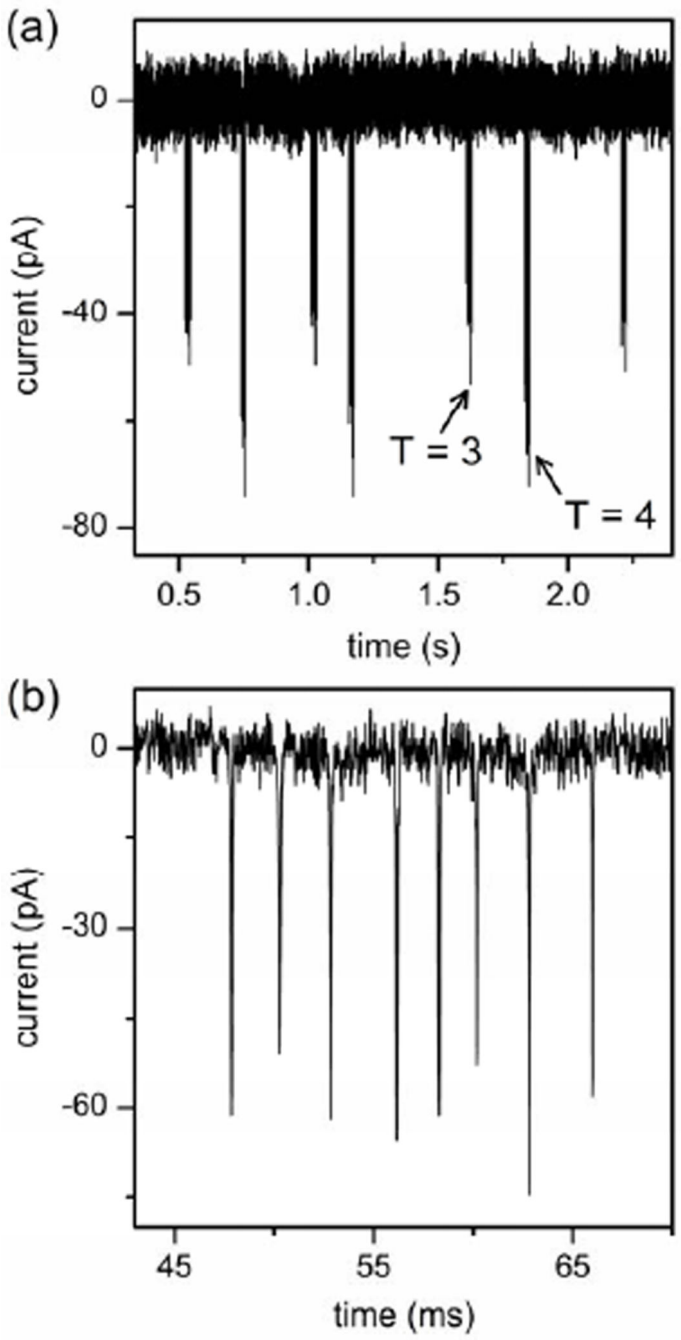

Figure 2.

(a) A 3-s current trace of a 1:1 mixture of T = 3 and T = 4 capsids measured on an 8-pore device. The smaller T = 3 capsid displaces a proportionally smaller amount of current than the larger T = 4 capsid. (b) Pulse sequence from the translocation of a single T = 4 capsid through an 8-pore device. The baseline current (~17 nA) has been subtracted from the signal.

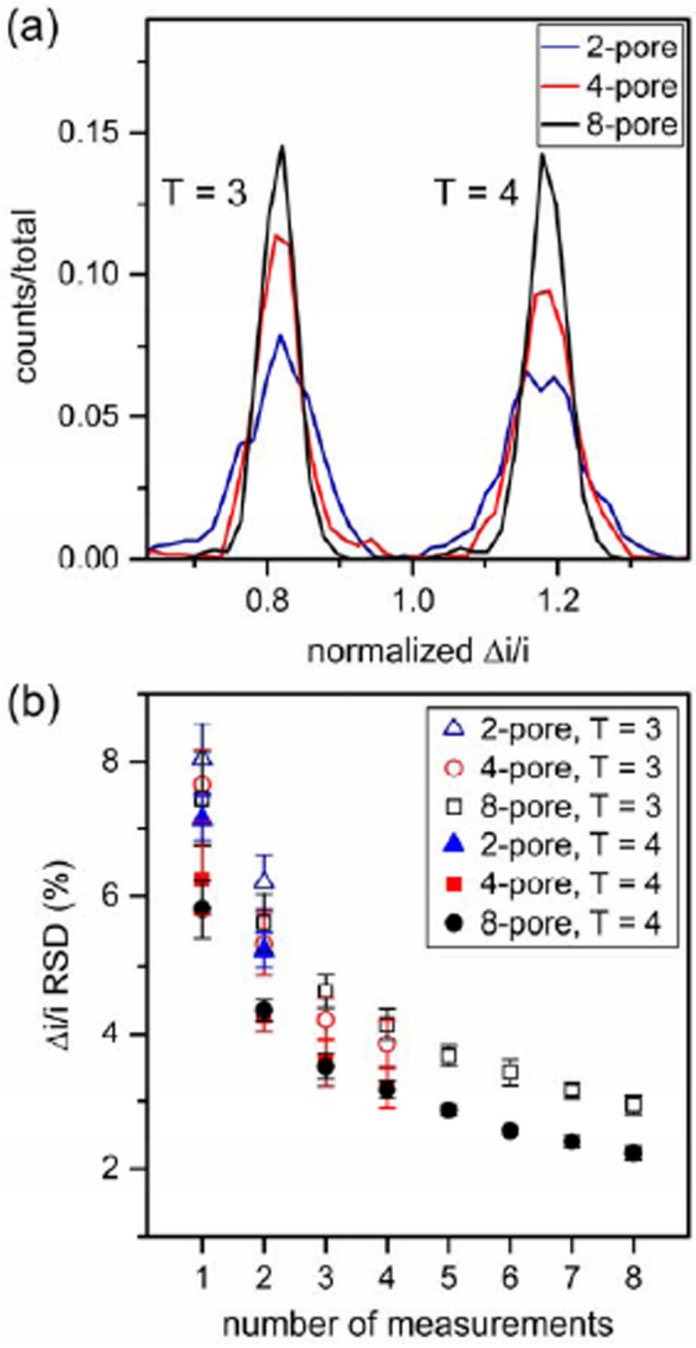

Figure 3.

(a) Histograms of normalized pulse amplitude (Δi/i) for a 1:1 mixture of T = 3 and T = 4 capsids measured on 2-, 4-, and 8-pore devices. To overlay the histograms, the x-axis was normalized by dividing the Δi/i by the average of the means of the pulse amplitude distributions for T = 3 and T = 4 capsids. (b) The relative standard deviation (RSD) of the pulse amplitude distributions for T = 3 and T = 4 capsids from 2-, 4-, and 8-pore devices. Measurements equivalent to 1, 1–3, and 1–7 averaged pulses were extracted from data from the 2-, 4-, or 8-pore devices, respectively.

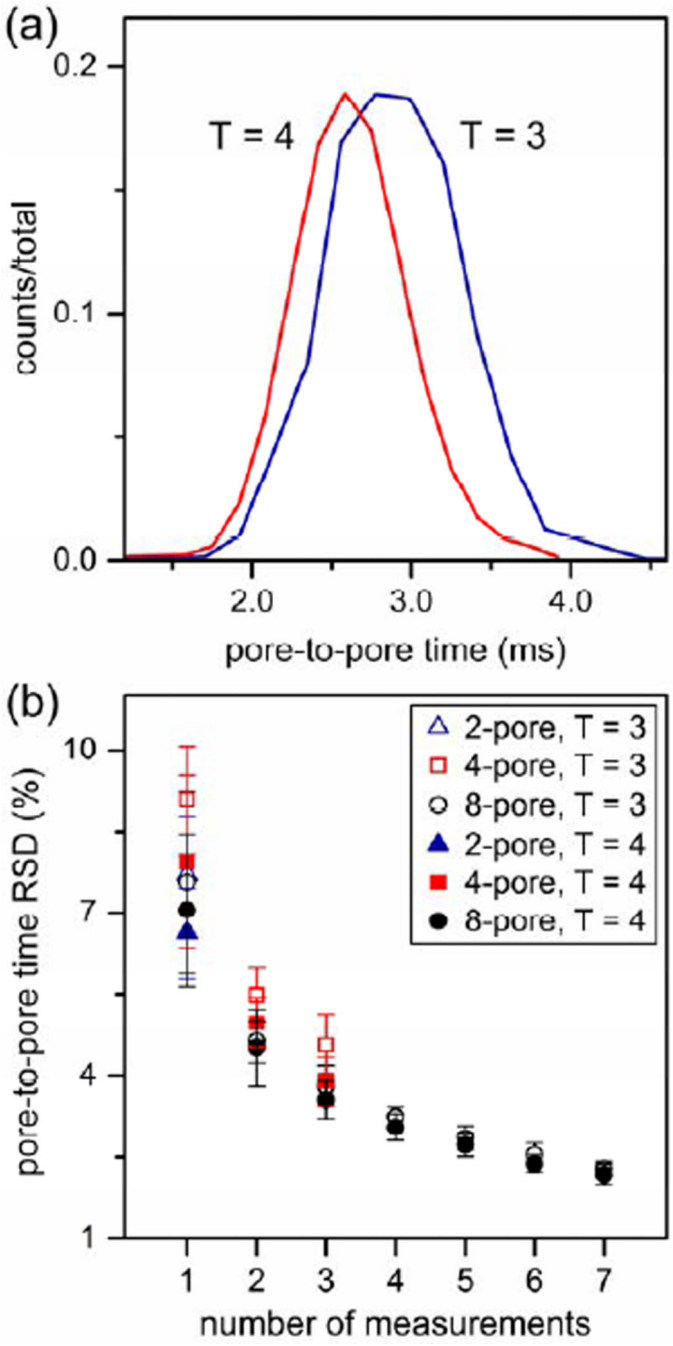

Figure 4.

(a) Histograms of the average pore-to-pore time for T = 3 and T = 4 capsids measured on an 8-pore device. T = 3 and T = 4 capsids have similar, but not identical electrophoretic mobilities. (b) Relative standard deviation (RSD) of the pore-to-pore time distributions for T = 3 and T = 4 capsids from 2-, 4-, and 8-pore devices. Measurements equivalent to 1–2 and 1–6 pore-to-pore times were extracted from data from the 4-and 8-pore devices, respectively.

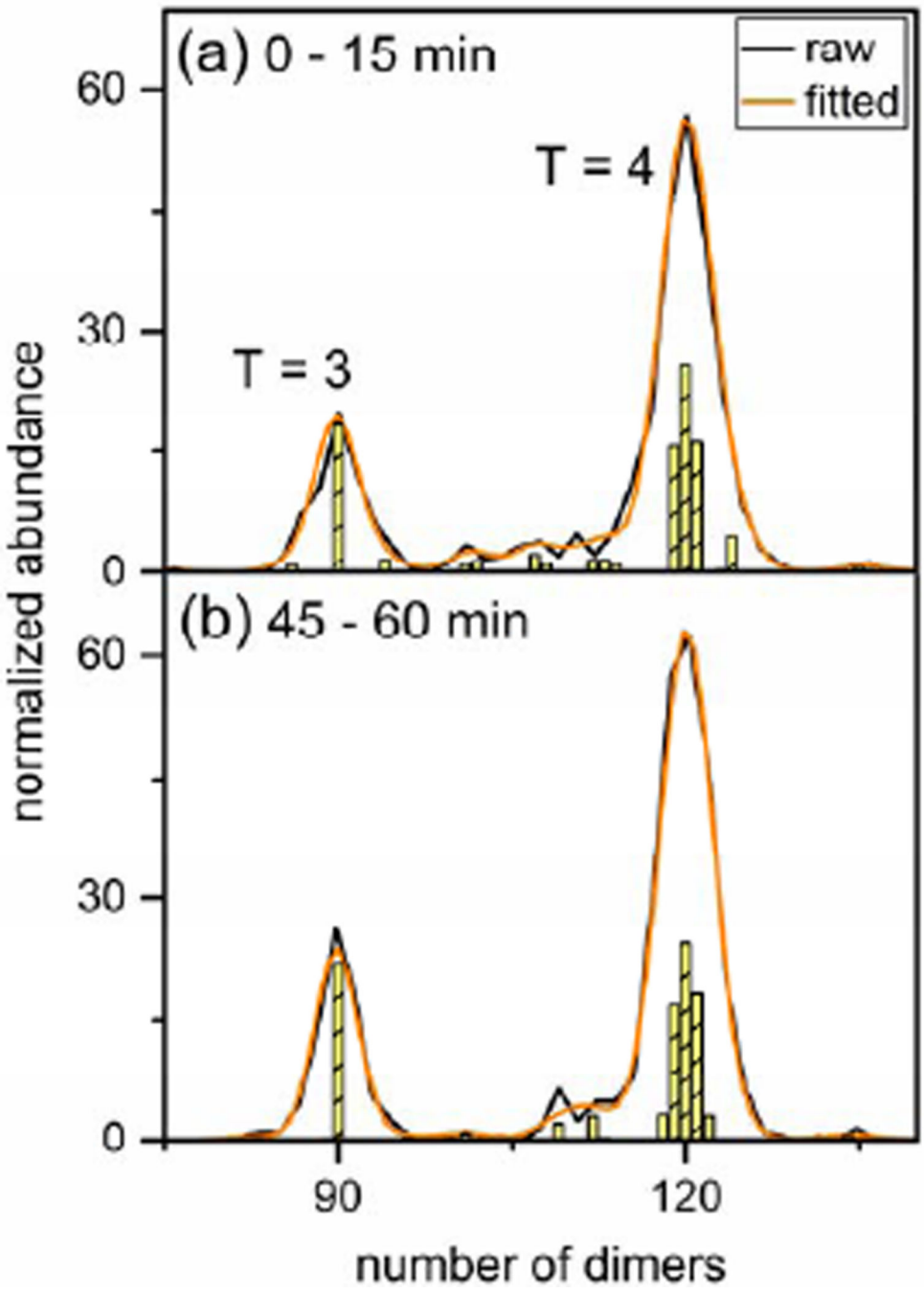

Figure 5.

Histograms of pulse amplitudes from (a) 0 to 15 min and (b) 45 to 60 min of a capsid assembly reaction of HBV. T = 3 capsids, T = 4 capsids, and intermediate species were assembled from 0.40 μM dimer in 1 M NaCl and measured with an 8-pore device. Overlaid are the raw data (black line) and corresponding fitted curve (orange line), and the yellow bars represent the means and amplitudes of the fitted Gaussian distributions. After the first 15 min, the concentration of intermediates from 92 to 104 dimers decreased significantly. Each histogram includes ~750 particles.

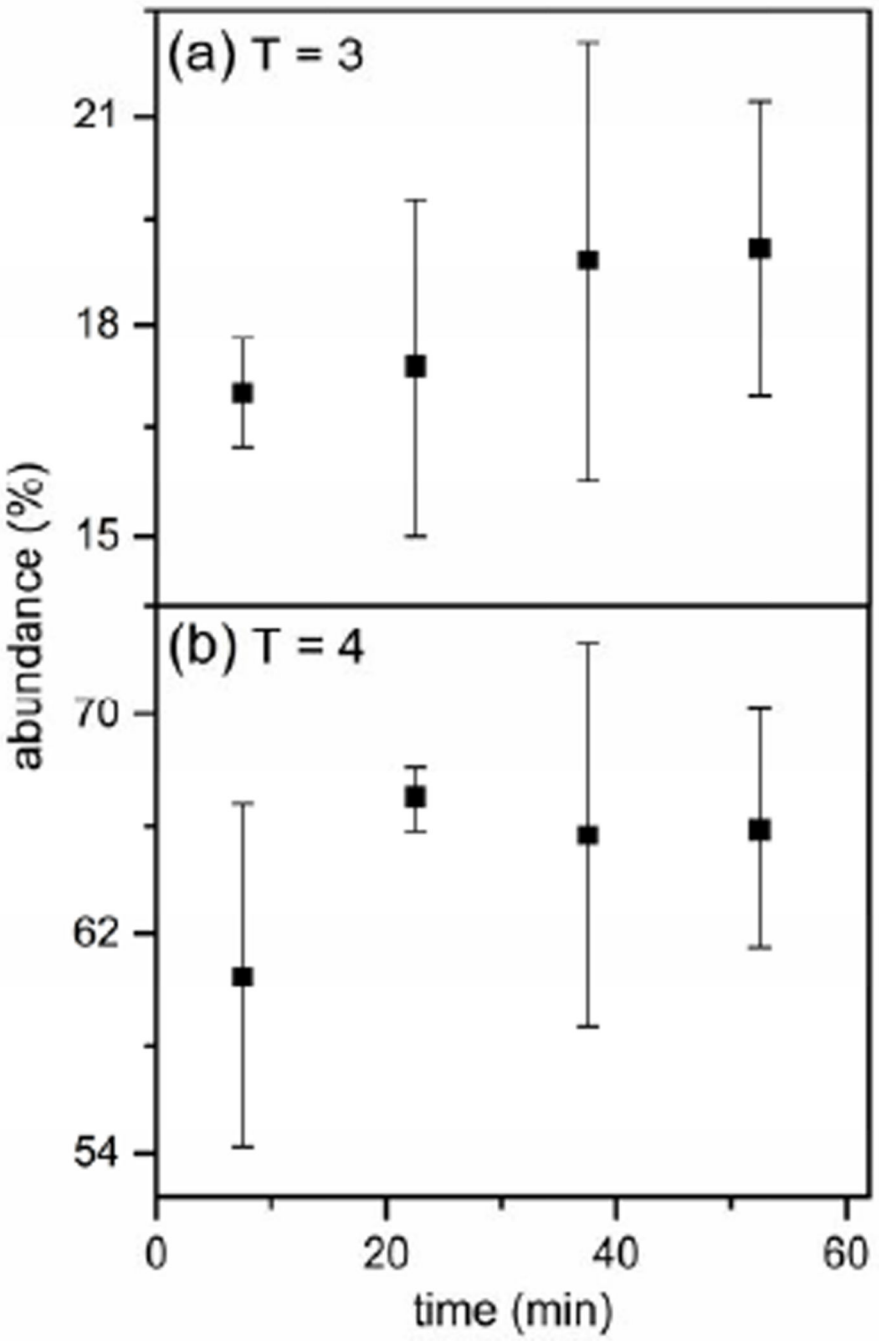

Figure 6.
Variation of the abundance of (a) T = 3 capsids (90 ± 1 dimer units) and (b) T = 4 capsids (120 ± 2 dimer units) with time for HBV assembly of 0.40 μM dimer in 1 M NaCl. The abundances of both T = 3 and T = 4 capsids increased slightly over time.

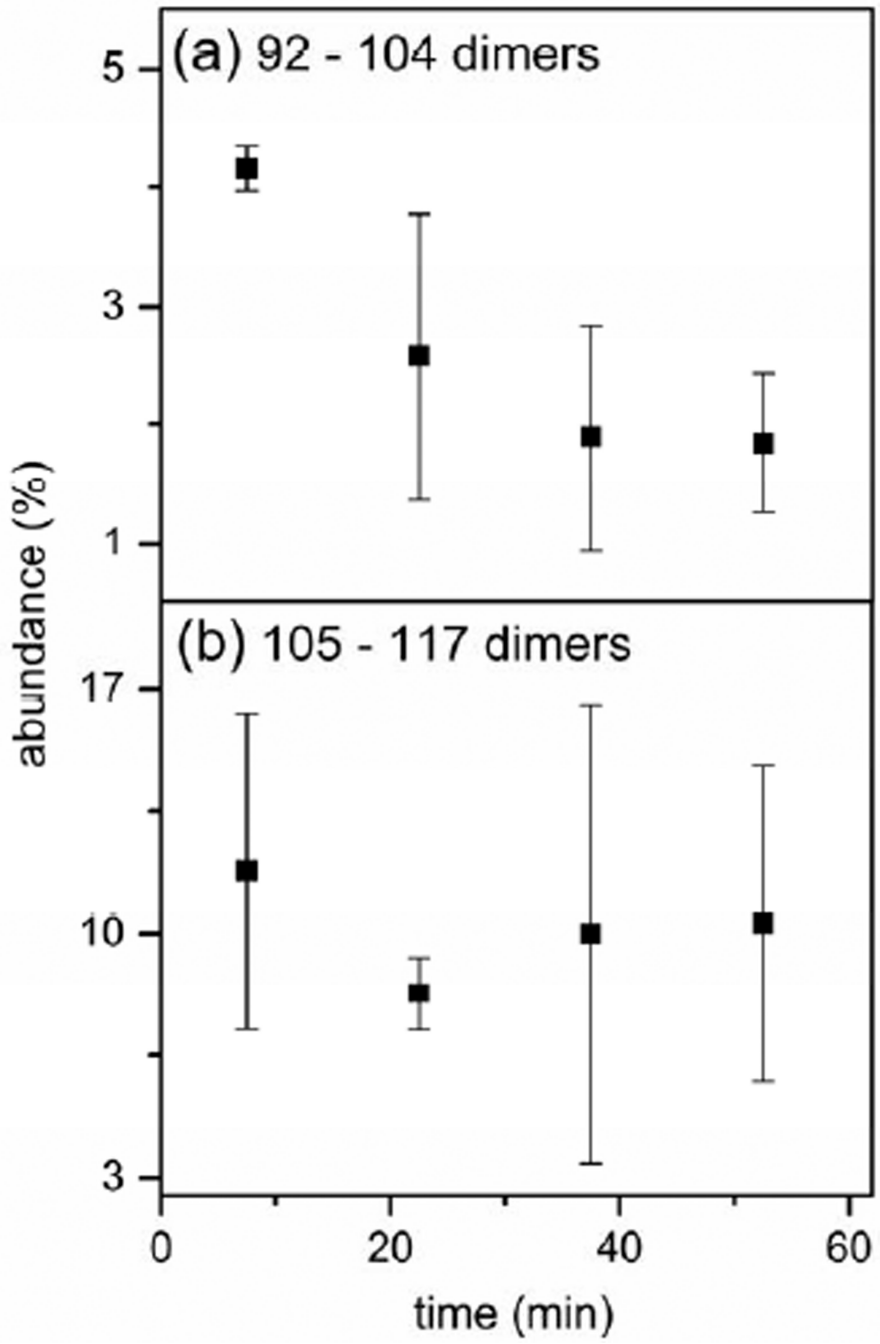

Figure 7.

Variation of the abundance of intermediates with (a) 92–104 dimers and (b) 105–117 dimers over time for HBV assembly of 0.40 μM dimer in 1 M NaCl. The abundance of intermediates with smaller sizes (92–104 dimers) decreased, whereas the abundance of intermediates with larger sizes (105–117 dimers) remained constant.